Ceramics International 45 (2019) 3510–3517

Contents lists available at ScienceDirect

Ceramics International

journal homepage: www.elsevier.com/locate/ceramint

Influence of deposition parameters on the structure and microstructure of $Bi_{12}TiO_{20}$ films obtained by pulsed laser deposition

L.F. Gorup[a,b,d], V. Bouquet[b], S. Députier[b], V. Dorcet[b], M. Guilloux-Viry[b], I.M.G. Santos[c], A.A. Silva[d], A.E. Nogueira[e], A.M. Kubo[a], E. Longo[a], E.R. Camargo[a,*]

[a] LIEC - Department of Chemistry, UFSCar-Federal University of São Carlos, Rod. Washington Luis km 235, CP 676, São Carlos, SP 13565-905, Brazil
[b] Institut des Sciences Chimiques de Rennes, UMR 6226 CNRS/Université de Rennes 1, Campus de Beaulieu, 35042 Rennes, France
[c] LACOM,, Department of Chemistry, Federal University of Paraiba, Campus I, CEP 58059-900, João Pessoa, PB, Brazil
[d] FACET – Department of Chemistry, Federal University of Grande Dourados, Dourados, MS 79804-970, Brazil
[e] Brazilian Nanotechnology National Laboratory (LNNano), Brazilian Center for Research in Energy and Materials (CNPEM), Zip Code 13083-970, Campinas, São Paulo, Brazil

ARTICLE INFO

Keywords:
$Bi_{12}TiO_{20}$ (BTO) thin films
Pulsed laser deposition
Metastable phases
Metastable phases
Morphology and surface roughness

ABSTRACT

The structure, morphology and surface roughness of $Bi_{12}TiO_{20}$ (BTO) thin films grown on R-sapphire by pulsed laser deposition (PLD) were studied at different substrate temperatures, target-substrate distances, oxygen pressures and laser-pulse repetition rates. Although the substrate temperature seems to be the most important experimental parameter, the gas pressure and the target–substrate distance played important role on the phase formed and film thickness, with a significant effect of the laser-pulse repetition rate on the films thickness and preferred orientation of the deposited film. Single-phase γ-$Bi_{12}TiO_{20}$ was obtained on substrates at 650 °C, while several BTO metastable phases were observed in films deposited on substrates at temperatures between 500 and 600 °C. By the first time, thin films of pure and textured δ-$Bi_{12}TiO_{20}$ were successfully growth on substrates at 450 °C. When annealed, all the films deposited at lower temperatures resulted in the thermodynamically stable γ-$Bi_{12}TiO_{20}$.

1. Introduction

Semiconductor photocatalysts for solar energy conversion is an active area in the field of environmental research. Although the development of various materials, the design of efficient visible light-driven photocatalysts is still a great challenge [1–7]. Bismuth titanate (BTO) is a promising candidate to replace TiO_2 because of its chemical stability, nontoxicity and enhanced photocatalytic reactivity. Bismuth oxide occurs in different composition and structures, such as $Bi_4Ti_3O_{12}$ [8–10], $Bi_2Ti_2O_7$ [11] $Bi_2Ti_4O_{11}$ [12], $Bi_{20}TiO_{32}$ [13–16] and $Bi_{12}TiO_{20}$ phase [3–5,17–21], but there are at least three polymorphs that exhibit catalytic properties [22–25] and unusual high photocatalytic activity under solar light irradiation [26–29]. The $Bi_{12}TiO_{20}$ belongs to the sillenite family, where the bismuth coordinates to five oxygens of the octahedra together with the stereochemically active 6 s2 lone electron pair of Bi^{3+}. This configuration turns this structure unique for application in photocatalysis. When synthesized as powders, two polymorphs were identified, the γ-$Bi_{12}TiO_{20}$ formed at room temperature and the δ-$Bi_{12}TiO_{20}$ that is stable only at high temperature [30–34]. The γ-$Bi_{12}TiO_{20}$ has the (BCC) body-centered cubic structure of γ-Bi_2O_3 (space group I23) while the δ-$Bi_{12}TiO_{20}$ have the (FCC) face-centered cubic structure of δ-Bi_2O_3 (space group *Fm*-3*m*). The γ-$Bi_{12}TiO_{20}$ showed the photocatalytic ability to degrade organic pollutants, offering a potentially efficient technology for the elimination of toxic waste chemicals [35–38]. Nanostructured γ-$Bi_{12}TiO_{20}$, for example, exhibited improved photoelectrochemical activity to generate hydrogen and to degrade textile dye under UV–visible light [39]. Indeed, γ-$Bi_{12}TiO_{20}$ powders exhibited superior performance than the commercial TiO_2 (P25 catalyst) under visible light irradiation [40,41] and could degrade dyes much more efficiently than the traditional N-doped TiO_2 [42].

Various methods have been used to synthesize sillenite γ-$Bi_{12}TiO_{20}$, such as chemical solution decomposition [21,43], isopropanol-assisted hydrothermal synthesis [2,41,42], coprecipitation [36,44], Pechini-based routes [45], electrochemical method [39,46], sol-gel processing [47], the traditional solid-state reaction [48] and, recently, by means of the oxidant peroxo method (OPM) [49–52].

Although several studies used ultrafine powders suspended in the

* Corresponding author.
E-mail address: camargo@ufscar.br (E.R. Camargo).

https://doi.org/10.1016/j.ceramint.2018.11.008
Received 23 September 2018; Received in revised form 2 November 2018; Accepted 2 November 2018
Available online 12 November 2018

reaction media, photocatalyst in the form of supported thin film provides an advantage over the drawbacks encountered in powder suspensions. In fact, there are only a few studies focused on the synthesis and applications of $Bi_{12}TiO_{20}$ thin films. [46,53–58]. In this context, it appears attractive to synthesize thin films of $Bi_{12}TiO_{20}$ with controlled structure and microstructure aiming applications in photocatalysis. This study presents the synthesis of $Bi_{12}TiO_{20}$ thin films growth by pulsed laser deposition (PLD) evaluating the influence of several experimental parameters, such as the control of the substrate temperature, oxygen pressure, target-substrate distance and the laser-pulse repetition frequency on the microstructural (thickness, morphology, crystallinity) and structural (orientation and phases) properties.

2. Experimental

The γ-$Bi_{12}TiO_{20}$ powders were prepared by solid-state reaction from the stoichiometric mixture of Bi_2O_3 (99% Prolabo-France) and TiO_2 (99.8% Alfa Aesar GmbH & Co KG-Karlsruhe) powders. This stoichiometric mixture were mixed in a planetary ball mill (Retsch-PM 100) with a rotational speed of 400 rpm for one hour, pressed uniaxially at 100 MPa in pellets and fired at 750 °C for 2 h. In a second step, the fired bismuth titanate was milled again using the planetary ball mill at 400 rpm for one hour, and the fine powder was pressed uniaxially at 100 MPa to form discs with diameters of 25 mm and thickness of 3 mm. These discs were sintered at 750 °C for 4 h to obtain dense ceramics of γ-$Bi_{12}TiO_{20}$ that were used as target for PLD deposition. Thin films of bismuth oxide were deposited on R-sapphire (Al_2O_3) single crystal substrate by PLD using a KrF excimer laser (Tuilaser Excistar, with pulse duration of 20 ns at $\lambda = 248$ nm) operating at 220 mJ (corresponding to a fluence of 2 J cm^{-2}). The deposition parameters are described in the Table SM1 of the Supplementary and are shown in Fig. 1. The temperature of R-sapphire substrate was controlled during the film growth using a thermocouple placed on the substrate holder, while the oxygen gas was introduced inside the deposition chamber at constant flux. The deposition was fixed at 15 min for all of the experiments.

The BTO thin films were characterized by X-ray diffraction (D8 Advanced Brüker AXS) in the θ–2θ mode with the monochromatized Cu Kα1 radiation. Surface morphology and thickness were determined by field-emission scanning electron microscopy (FE-SEM) using a JEOL JSM 6310F system working at a low accelerating voltage (7 kV) in order to limit the charge effects and to achieve a high resolution. The composition of films was analyzed by energy-dispersive X-ray spectroscopy (EDS) using a JEOL JSM 6400 scanning electron microscope equipped with an ISIS Oxford analyzer (10 kV was used as an accelerating voltage and 10 nA as a beam current). Lattice parameters were determined from the X-ray diffraction (XRD) patterns. Surface morphology of selected samples was analyzed by atomic force microscopy (AFM) using a SPM 5500-Agilent operating in tapping mode with a scanning frequency of 1 Hz. The measured root mean square (RMS) roughness of surfaces was calculated from the AFM images. Catalytic performance of some BTO powders synthesized by solid state reaction at different temperatures (500–750 °C) were also evaluated during the photocatalytic degradation of rhodamine B under ultraviolet radiation and are presented in the supplementary material.

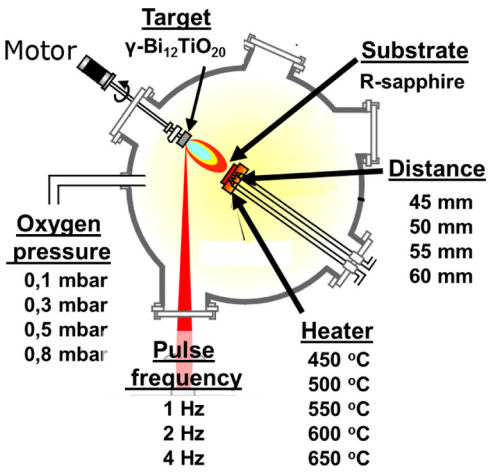

Fig. 1. Experimental parameters used to obtain the BTO thin films by PLD. The films were deposited on substrates of R-sapphire at different temperatures, evaluating the influence of the oxygen pressure, the distance between the target and the substrate and the laser-pulse repetition frequency. All the depositions occurred during 15 min.

3. Results and discussion

There are several experimental parameters controlling the growth of $Bi_{12}TiO_{20}$ films deposited by PLD. Nevertheless, each parameter was analyzed separately in this study in order to determine its influence either in the crystalline structure or in the microstructure of the BTO deposited film. Among all the parameters, substrate temperature seems to be the most important variable to control the crystalline structure and preferred orientation, while oxygen pressure and target–substrate distance played an important role in the phase formed and film thickness. The laser-pulse repetition frequency also showed a significant effect on the films thickness and on the preferred orientation of the deposited material.

3.1. Temperature of the R-sapphire substrate

Fig. 2 shows XRD patterns of $Bi_{12}TiO_{20}$ thin films deposited on R-sapphire substrates at different nominal temperatures, which appears to be the key parameter to control the crystallinity of BTO system. All the films deposited were polycrystalline, in spite the fact that some of them exhibited preferential orientation. The peaks assigned with ✱

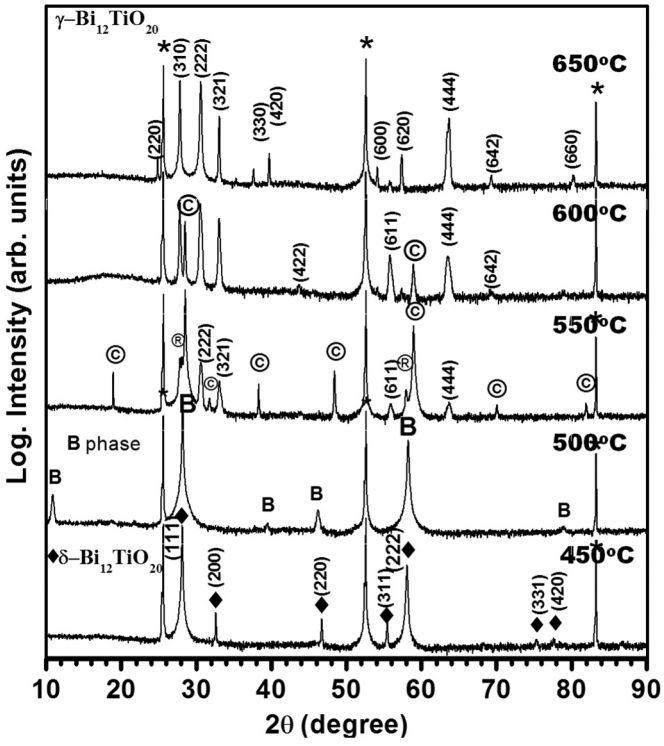

Fig. 2. X-ray patterns of thin films deposited on substrates at different temperatures. All the experiments were performed at constant laser-pulse repetition rate of 2 Hz, oxygen pressure of 0.5 mbar and target-substrate distance of 55 mm. The δ-$Bi_{12}TiO_{20}$ phase is assigned with ♦. Unknown BTO phases are assigned by B, © and ® and the peaks assigned with ✱ belong to the substrate.

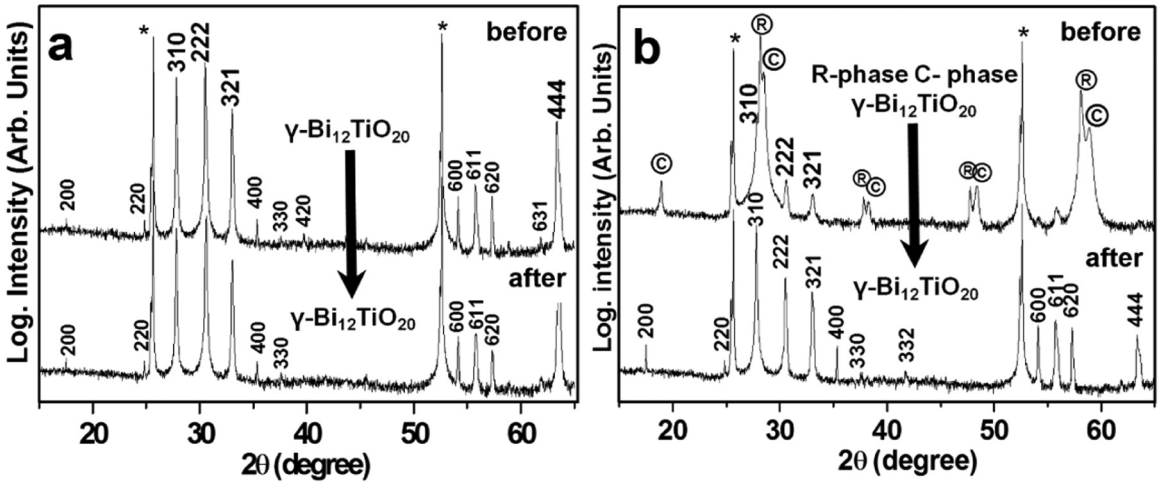

Fig. 3. X-ray patterns of the BTO thin films before and after annealing at 700 °C for 2 h. The XRD patterns in (a) show that thermodynamically stable γ-$Bi_{12}TiO_{20}$ is unaffected the annealing, while the metastable phases (b) are transformed to the γ-$Bi_{12}TiO_{20}$ phase after the treatment.

originated from the substrate and could be used to normalize the relative intensities. Although the films showed a mixture of phases when deposited at temperatures up to 600 °C, single-phase BCC γ-$Bi_{12}TiO_{20}$ (PDF 34–0097) were successfully obtained when the films were deposited on substrates at 650 °C. The films deposited at temperatures between 550 and 600 °C, on the other hand, showed the secondary metastable C and R phases. A third unknown phase (indicated with B) was observed in the films deposited at 500 °C. For sake of clearness, the intensities of the diffraction peaks are in logarithmic scale. For this reason, their use to evaluate the relative amounts of each phase should be done with care. It is interesting to note the single-phase FCC δ-$Bi_{12}TiO_{20}$ (PDF 42–0186) formed at 450 °C with preferential orientation, as indicated by the anomalously intense peaks (111) and (222). Indeed, the XRD pattern of δ-$Bi_{12}TiO_{20}$ in Fig. 2 is the very first report about the thin films of δ-$Bi_{12}TiO_{20}$ growth by PLD. Trials to reduce the deposition temperature below than 450 °C also resulted in single-phase of δ-$Bi_{12}TiO_{20}$ but with a huge amount of amorphous material. Further experiments to evaluate the thermal stability of the metastable phases (δ, C, R and B) resulted in films of the thermodynamically stable γ-$Bi_{12}TiO_{20}$ phase upon annealing at 700 °C for 2 h (Fig. 3).

Although only a few studies focused the phase transition in the BTO system, it can be compared with the isostructural Bi_2O_3-SiO_2 system [48]. Fig. 4 shows the similarities and differences between the metastable phases of the BTO thin films deposited by PLD on R-sapphire and the Bi_2O_3 and $Bi_{12}TiO_{20}$ powders synthesized by the solid-state reaction and thin films of Bi_2O_3 growth by sputtering [25,59]. It is worth to note that both BTO and Bi_2O_3 powders exhibited the isostructural metastable phases δ-$Bi_{12}TiO_{20}$ and δ-Bi_2O_3 at higher temperatures. It is the contrary of observed in the films, where the δ-phases appear only at lower substrate temperatures, although the δ-$Bi_{12}TiO_{20}$ film were transformed in the more stable γ-$Bi_{12}TiO_{20}$ phase after an appropriate annealing treatment. The Fig. 4 suggests a different crystallization path for the films (δ → B → C → γ for the BTO system synthesized by PLD, and R → γ for the Bi_2O_3 prepared by sputtering) than that observed during the synthesis of powders. In this context, the δ-$Bi_{12}TiO_{20}$ phase seems to be kinetically favored during the growth of films, while the γ-$Bi_{12}TiO_{20}$ is the thermodynamically stable phase. Our experiments about the thermal stability of the metastable phases corroborated this result. Similar event was observed during the transition α-Bi_2O_3 → δ-Bi_2O_3 of thin films prepared by sputtering, where the metastable phases (β, γ, ω, ε and δ) transformed in the predominant thermodynamically stable α-Bi_2O_3 phase after annealing [25,59].

The classical approach to solve the problem of nucleation is considering the deposition of dissimilar materials as a heterogeneous nucleation event, generally discussed in terms of the Volmer-Weber mechanism [9,60]. The SEM images of Fig. 5 show films at different growth evolution stages in function of the substrate temperature, from the equiaxed islands in the films deposited at 450 and 500 °C to the elongated and percolated morphologies in the films deposited at 550 and 600 °C. The γ-$Bi_{12}TiO_{20}$ film formed at 650 °C presents a smooth surface, characteristic of the final step of the growth process, including the presence of some isolated holes [61,62].

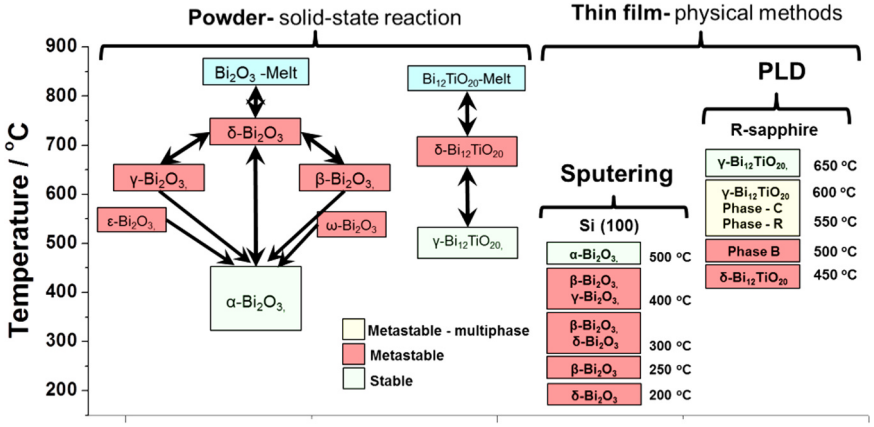

Fig. 4. Scheme comparing the matastable phases of Bi_2O_3 and $Bi_{12}TiO_{20}$ powders synthesized by the traditional solid state reaction (Mehring 2007) and thin films deposited by sputtering (Fan 2006) and PLD (this study).

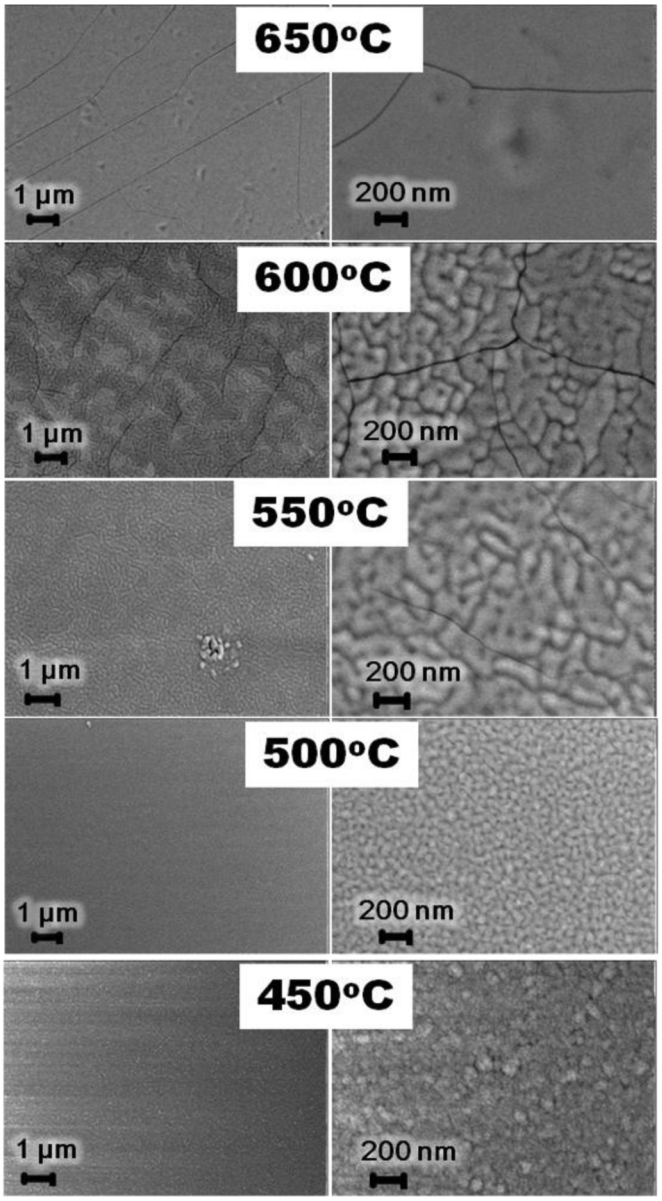

Fig. 5. SEM images of the films deposited on the substrate at different temperatures. All the experiments were performed at constant laser-pulse repetition rate of 2 Hz, oxygen pressure of 0.5 mbar and a target-substrate distance of 55 mm.

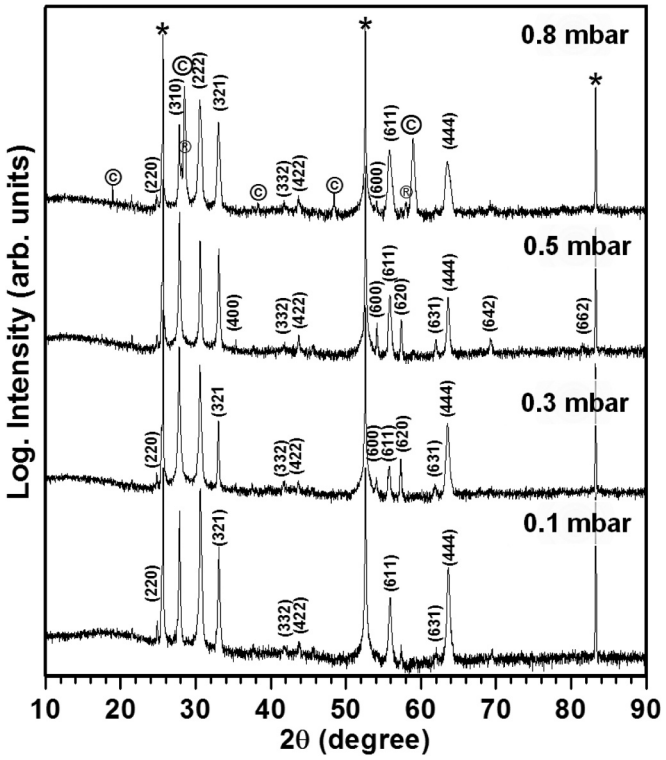

Fig. 7. X-ray patterns of thin films deposited on substrates at different oxygen pressures. All the experiments were performed at constant laser-pulse repetition rate of 2 Hz, target-substrate distance of 55 mm and substrate temperature of 600 °C. The γ-$Bi_{12}TiO_{20}$ phase is assigned with the Miller indexes and the matastable phase is indicated by ©. The peaks assigned with ✱ belong to substrate.

The AFM image of the film deposited at 650 °C (Fig. 6a) shows a RMS roughness height of 114 nm while the much smoother film deposited at 450 °C (Fig. 6b) exhibited a roughness of 64 nm, which is in agreement with the expected rougher films at final stages of the growth mechanism [62]. The substrate temperature plays an important role in determining the critical size of cluster during the nucleation step. At lower temperatures, the binding energy is sufficiently high to stabilize small clusters of different structures, even when they are thermodynamically unstable [60]. At higher temperatures, on the other hand, only a few structures of high stability are allowed to grow. As mentioned earlier (Fig. 2), the films deposited at 450 °C resulted in the preferentially orientated δ-$Bi_{12}TiO_{20}$, while the thermodynamically stable γ-$Bi_{12}TiO_{20}$ phase was obtained at higher temperature.

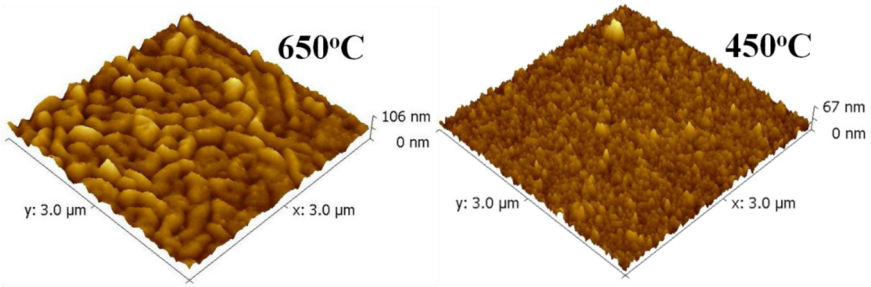

Fig. 6. AFM images of the $Bi_{12}TiO_{20}$ thin films deposited at 650 °C and 450 °C. The experiments were performed at constant laser-pulse repetition rate of 2 Hz, oxygen pressure of 0.5 mbar and target-substrate distance of 50 mm.

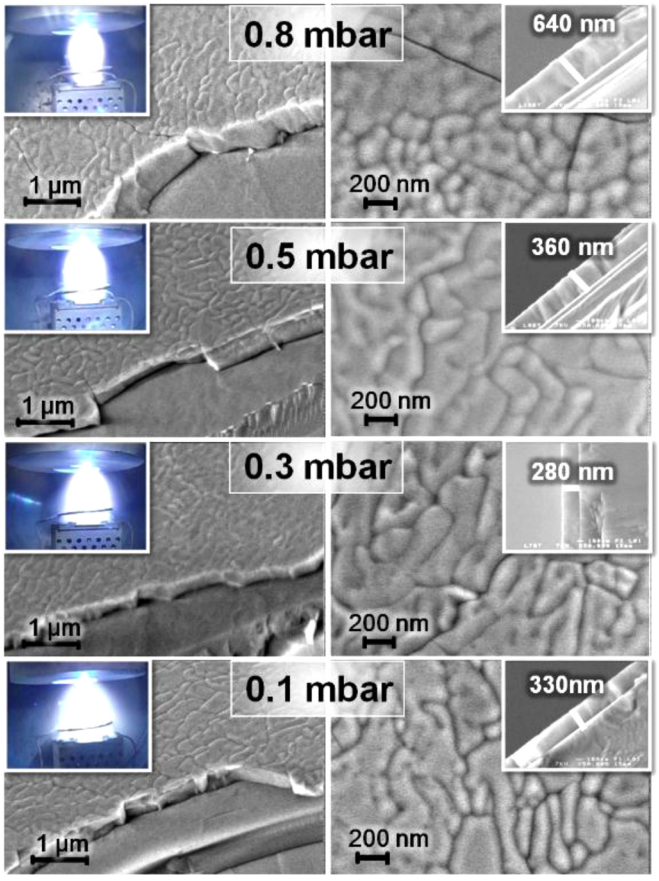

Fig. 8. SEM images of thin films deposited at different oxygen pressures. All the experiments were performed at constant laser-pulse repetition rate of 2 Hz, target-substrate distance of 50 mm and substrate temperature of 600 °C. The details show the respective plasma plume and the film thickness.

The growth mechanism can be described in the following steps: (i) nucleation, (ii) growth and coalescence, (iii) channel development and (iv) the filling of remaining holes (Bask1994). Therefore, once the small nuclei of the kinetically favored δ-$Bi_{12}TiO_{20}$ phase are formed on the substrate at lower temperatures, they can grow feed by the deposit flux generated by the pulsed laser on the surface of the target, resulting in a uniform morphology of small preferentially orientated grains of δ-$Bi_{12}TiO_{20}$ observed in Fig. 6b. However, when the substrate is heated, only larger nuclei of the stable γ-$Bi_{12}TiO_{20}$ phase can grow. It delays the growth mechanism favoring the coalescence of the isolated islands, which result in the random elongated morphology observed in Fig. 6a.

3.2. Deposition oxygen pressure

The reactive oxygen pressure acts as a striking parameter in the crystallinity and microstructure of the films. The Fig. 7 shows films of γ-$Bi_{12}TiO_{20}$ deposited on substrates at 600 °C under different oxygen pressures, without any evidence of preferred orientation. The secondary metastable C-phase was identified in the film prepared at 0.8 mbar of oxygen, confirming the dependence of the crystalline quality with the oxygen pressure and the influence of the substrate temperature on the films characteristics. The SEM images of Fig. 7 clearly show the dependence of thickness with the oxygen pressure, without pores, cracks or failures. Films deposited at 0.8 mbar exhibited a thickness of 640 nm,

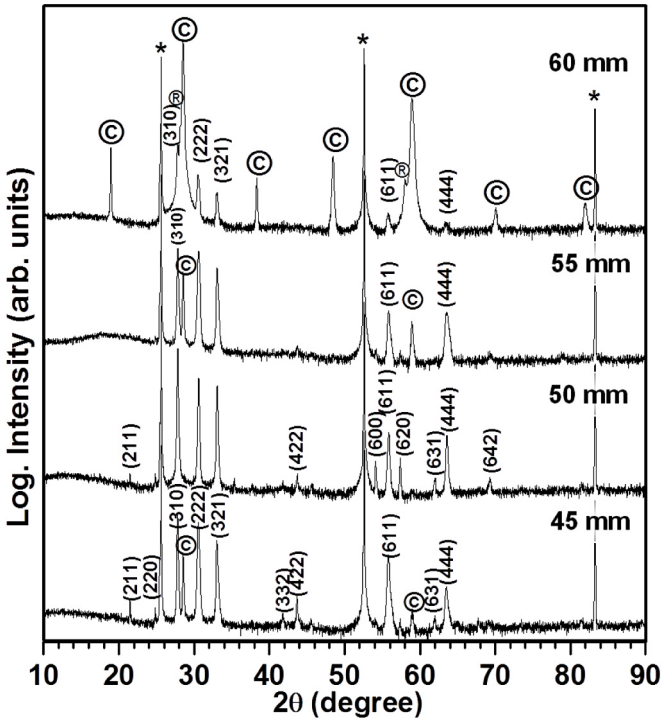

Fig. 9. X-ray patterns of thin films deposited on substrates at different target-substrate distances. All the experiments were performed at constant laser-pulse repetition rate of 2 Hz, substrate temperature of 600 °C and oxygen pressure of 0.5 mbar. The γ-$Bi_{12}TiO_{20}$ phase is assigned with the Miller indexes and the matastable phase is indicated by ©. The peaks assigned with ✱ belong to substrate.

which is almost the double of value observed in the films growth under a smaller pressure (0.1 mbar), suggesting that once determined the best temperature to crystallize a specific phase, the oxygen pressure can be tuned to control the final film thickness.

The insets on the top left corner of each SEM image of Fig. 8 show the dependence of the plasma plume shape with the oxygen pressure. As higher the pressure lower is the plasma plume dimension due to the gas compression, in agreement with previous Monte Carlo simulations [63–65]. Due to this effect, the density of the ablated species inside the plume should be higher at higher oxygen pressures, which modifies the material flux on the substrate. Since all substrates were exposed to the flux during the same time (15 min), thicker films were formed under higher oxygen pressures in consequence of the higher flux. Moreover, the synthesis of BTO films is hampered by the volatility of bismuth at the required temperature, however increasing the pressure outside of plume seems to favor the control of film composition.

3.3. The target-substrate distance

The target–substrate (T-S) distance appears to control phase, thickness and morphology of BTO films, which is related to the plasma dynamics occurring within the laser plume [66]. To evaluate its influence, several samples were prepared at T-S distances varying from 45 to 60 mm. The Fig. 8 shows their respective XRD patterns, recalling again the logarithm scale of the diffraction intensities. Although the existence of an empirical scaling law correlating the oxygen pressure and the target-substrate distance [67], all the experimental parameters except the distance were kept constant. The greater the distance most intense were

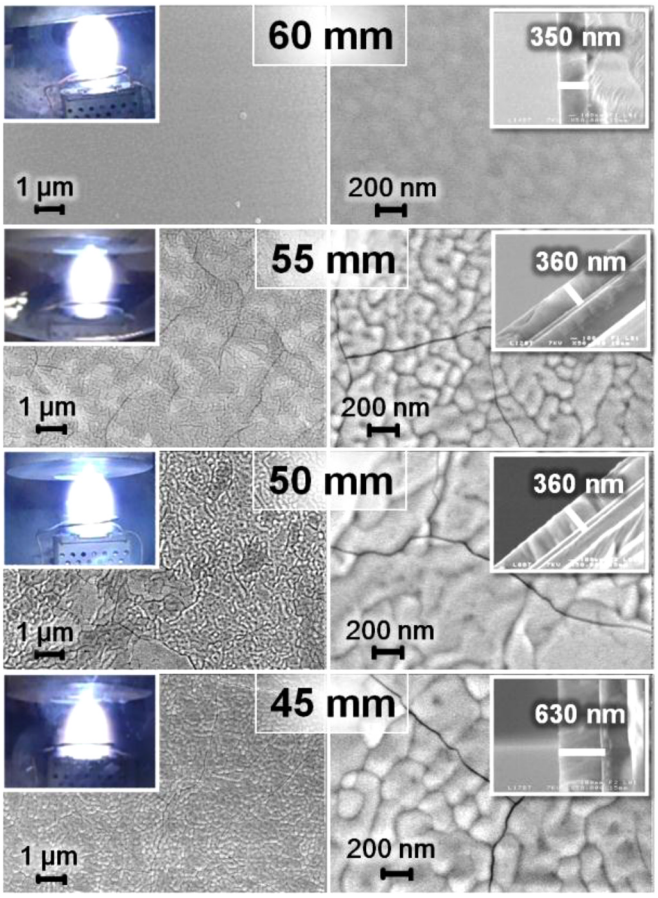

Fig. 10. SEM images of thin films deposited at different target-substrate distances. All the experiments were performed at constant laser-pulse repetition rate of 2 Hz, oxygen pressure of 0.5 mbar, target-substrate distance of 50 mm and substrate temperature of 600 °C. The details show the respective plasma plume and the film thickness.

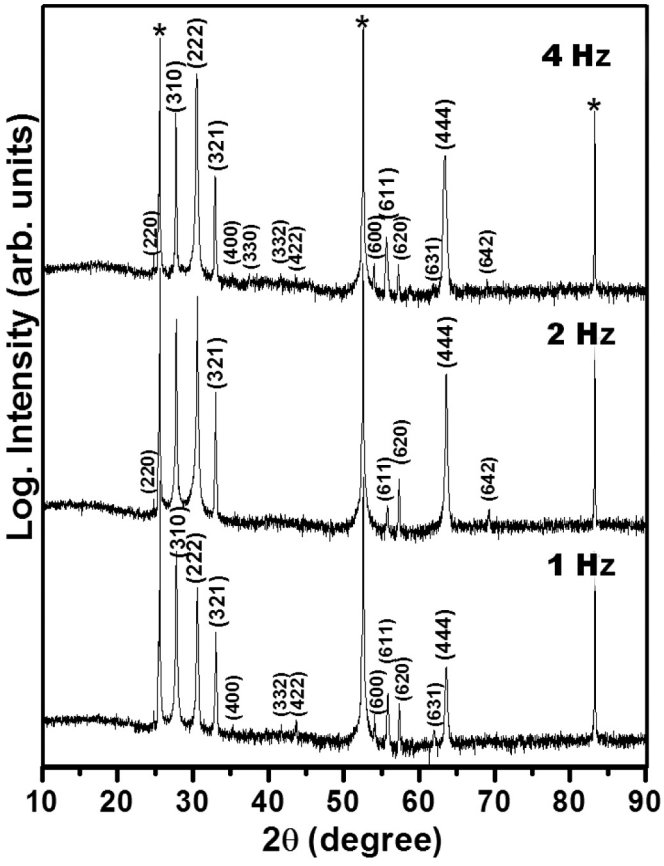

Fig. 11. X-ray patterns of thin films deposited on substrates at different laser-pulse repetition rates. All the experiments were performed with the substrates temperature at 600 °C, target-substrate distance of 55 mm and oxygen pressure of 0.3 mbar. The γ-$Bi_{12}TiO_{20}$ phase is assigned with the Miller indexes and the matastable phase is indicated by ©. The peaks assigned with ✱ belong to substrate.

the peaks of the C-phase compared to the peaks of γ-$Bi_{12}TiO_{20}$ nearly in all XRD patterns of Fig. 9. For instance, the peak of the C-phase at 28° in the film deposited on the substrate at 60 mm from target is almost one hundred times more intense than the peak (310) of the γ-$Bi_{12}TiO_{20}$. Moreover, the intense peaks (310), (222) and (321) of the γ-$Bi_{12}TiO_{20}$ suggest a preferential orientation at shorter distances, which corroborates the strong dependence between the oxygen pressure and the T-S distance. The important point is that there is not a universal optimum pressure to obtain films of high quality due to its dependence with the target-substrate distance. The SEM images of Fig. 10 show how the T-S distance affected the film thickness, which was reduced with the increase of target-substrate distance, from 630 nm of the film deposited at 45 mm to 350 nm for the film obtained at the distance of 60 mm. The images show the plume touching the surface of the substrate at short distances, which affects the material flux. The material flux of the ablated species in the plume decreases increasing the T-S distance, which lowers the deposition rate of the films and hence their thickness. As consequence, the composition of films deposited inside the plume is different from that formed outside, which also explains the differences on the morphology when the films were growth at different T-S distance.

3.4. Laser-pulse repetition rate

The laser-pulse repetition rate (LPRR) affects the thickness and the preferred orientation. Among the different LPRR frequencies tested, the deposition at 1 Hz resulted in textured films with the most intense peak (310) of the γ-$Bi_{12}TiO_{20}$ (Fig. 10). Please note the peaks with ✱ of the sapphire substrate. On the other hand, the most intense peak (222) appears in the film deposited at 4 Hz. Faster frequencies resulted in denser plumes, which obviously increased the film growth rate (Fig. 11) [68]. A linear dependence was observed between the thickness and the frequency. For instance, the film fabricated at 1 Hz exhibited a thickness of 150 nm after 15 min of exposition, compared to 440 nm of the film growth at 4 Hz (Fig. 12). Clearly, the LPRR strongly affects the morphology of the film since it also affects the nucleation rate on the substrate surface, resulting in different morphologies.

4. Conclusions

Although the compositional complexity, thin films of $Bi_{12}TiO_{20}$ were successfully obtained by pulsed laser deposition on R-sapphire substrates. Among all the experimental parameters studied, the substrate temperature affected the crystalline structure and preferred orientation, in spite the fact that gas pressure and the target–substrate distance played important role on the phase formed and film thickness. The laser-pulse repetition rate also showed a significant effect on the films thickness and on the preferred orientation of the deposited material. By adjusting the experimental conditions, the thermodynamically stable γ-$Bi_{12}TiO_{20}$ phase was formed on substrates at higher temperatures (650 °C), while the metastable δ-$Bi_{12}TiO_{20}$ could be obtained by the very first time at lower temperatures (450 °C). It was observed that the oxygen pressure could be used to control the film thickness of specific crystalline phase, since the optimum condition for high quality films depends on the target-substrate distance and laser-pulse repetition rate.

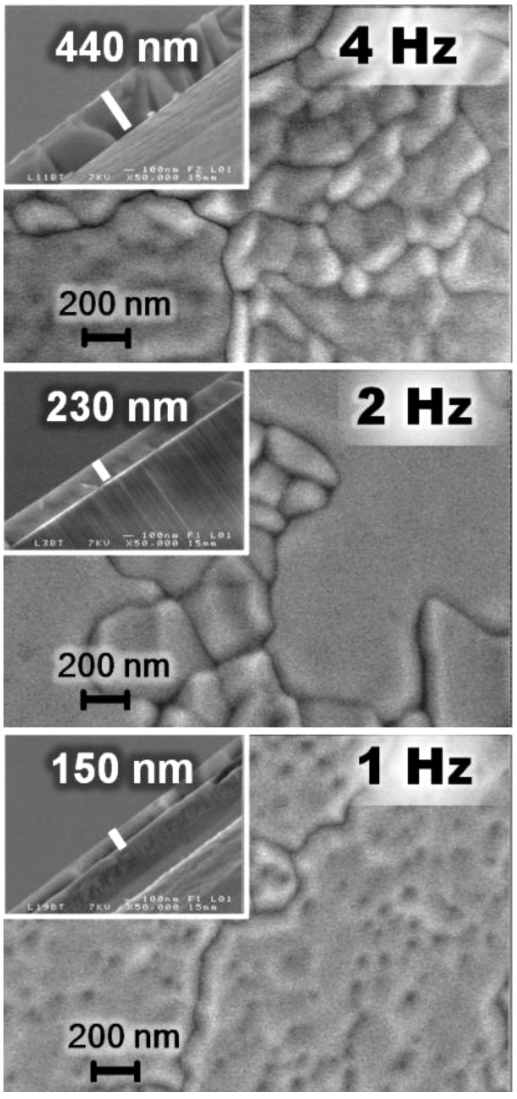

Fig. 12. SEM images of thin films deposited at different at different laser-pulse repetition rates. All the experiments were performed with the substrates temperature at 600 °C, target-substrate distance of 55 mm and oxygen pressure of 0.5 mbar. The details show the film thickness.

Acknowledgments

Authors acknowledge São Paulo Research Foundation/Brazil (Grant numbers 2012/07067-0, and 2013/07296-2), CNPq/Brazil and France-Brazil project (CAPES/ COFECUB n° 644/09) for financial support and the staff of CMEBA-France (ScanMAT, University of Rennes 1), which received a financial support from the European Union (CPER-FEDER 2007-2014), for the FE-SEM images.

In particular, we would like to acknowledge CEPID-Brazil (2013/07296-2) INCTMN 2008/57872-1 and CNPq 573636/2008-7. Special thanks to J. Le Lannic, Sophie Ollivier and Francis Gouttefangeas.

References

[1] G. Fang, L. Wang, G. Zhang, X. Yan, D. Wang, Rapid microwave-assisted sol-gel synthesis and exceptional visible light photocatalytic activities of Bi12TiO20, Ceramics International, 2018.
[2] J. Hou, Z. Wang, S. Jiao, H. Zhu, 3D Bi12TiO20/TiO2 hierarchical heterostructure: synthesis and enhanced visible-light photocatalytic activities, J. Hazard. Mater. 192 (2011) 1772–1779.
[3] Y. Nan, D. Yang, Z. Tong, Y. Sun, Z. Jiang, Fabrication of nanoplate-like g-C3N4/Bi12TiO20 heterojunction with enhanced visible-light photocatalytic activity, Mater. Res. Bull. 93 (2017) 91–101.
[4] R. Skiker, M. Zouraibi, M. Saidi, K. Ziat, Facile coprecipitation synthesis of novel Bi12TiO20/BiFeO3 heterostructure serie with enhanced photocatalytic activity for removal of methyl orange from water, J. Phys. Chem. Solids 119 (2018) 265–275.
[5] H. Sun, J. Li, G. Zhang, N. Li, Microtetrahedronal Bi12TiO20/g-C3N4 composite with enhanced visible light photocatalytic activity toward gaseous formaldehyde degradation: facet coupling effect and mechanism study, J. Mol. Catal. A: Chem. 424 (2016) 311–322.
[6] M.-S. Gui, W.-D. Zhang, Q.-X. Su, C.-H. Chen, Preparation and visible light photocatalytic activity of Bi2O3/Bi2WO6 heterojunction photocatalysts, J. Solid State Chem. 184 (2011) 1977–1982.
[7] W. Guo, Y. Yang, Y. Guo, Y. Jia, H. Liu, Y. Guo, Self-assembled hierarchical Bi12TiO20-graphene nanoarchitectures with excellent simulated sunlight photocatalytic activity, Phys. Chem. Chem. Phys. 16 (2014) 2705–2714.
[8] X. Lin, P. Lv, Q. Guan, H. Li, H. Zhai, C. Liu, Bismuth titanate microspheres: directed synthesis and their visible light photocatalytic activity, Appl. Surf. Sci. 258 (2012) 7146–7153.
[9] K. Sardar, R.I. Walton, Hydrothermal synthesis map of bismuth titanates, J. Solid State Chem. 189 (2012) 32–37.
[10] L. Wiehl, A. Friedrich, E. Haussuehl, W. Morgenroth, J. Biehler, B. Winkler, M. Hanfland, High pressure powder X-ray diffraction of sillenites Bi12MO20 (M = Si, Ge, Ti) and Bi4Ti3O12, J. Solid State Chem. 208 (2013) 35–42.
[11] W. Yao, Photocatalytic property of bismuth titanate Bi2Ti2O7, Appl. Catal. A: General. 259 (2004) 29–33.
[12] T. Kidchob, L. Malfatti, D. Marongiu, S. Enzo, P. Innocenzi, Sol-gel processing of Bi2Ti2O7 and Bi2Ti4O11 films with photocatalytic activity, J. Am. Ceram. Soc. 93 (2010) 2897–2902.
[13] L. Zhang, X. Zhang, Y.-Q. Huang, C.-L. Pan, J.-S. Hu, C.-M. Hou, Novel Bi12ZnO20-Bi2WO6 heterostructures: facile synthesis and excellent visible-light-driven photocatalytic activities, RSC Adv. 5 (2015) 30239–30247.
[14] Y. Hou, M. Wang, X. Xu, H. Wang, S. Shang, D. Wang, W. Yao, Bi20TiO32 nanocones prepared from Bi–Ti–O mixture by metalorganic decomposition method, J. Cryst. Growth 240 (2002) 489–494.
[15] X. Sun, L. Sun, H. Zhang, J. Ma, Preparation of visible-light responsive photocatalyst (bi20tio32) and its photocatalytic activity for degrading organic pollutants, in: Proceedings of the 2009 International Conference on Energy and Environment Technology - Volume 01, IEEE Computer Society, 2009, pp. 253–256.
[16] H. Cheng, B. Huang, Y. Dai, X. Qin, X. Zhang, Z. Wang, M. Jiang, Visible-light photocatalytic activity of the metastable Bi20TiO32 synthesized by a high-temperature quenching method, J. Solid State Chem. 182 (2009) 2274–2278.
[17] X. Li, Z. Song, N. Su, Effect of electrolyte component on the synthesis of bismuth titanate by the anodic spark conversion method, Optik 136 (2017) 192–197.
[18] P. Petkova, K. Boubaker, P. Vasilev, M. Mustafa, A. Yumak, D. Bachvarova, Common and different doping patterns within photo-reactive complexes of Co2+ in Bi12SiO20 and Co3+ in Bi12TiO20, Opt. - Int. J. Light Electron Opt. 127 (2016) 3925–3928.
[19] Y. Wang, Y. Zhang, L. Yan, J. Li, C. Wang, F. Fu, A novel magnetically recyclable photocatalyst of Bi12TiO20/Co composites with enhanced photocatalytic performance, Ceram. Int. 43 (2017) 15965–15969.
[20] L.H. Wang, M.L. Zhao, C.L. Wang, J. Wang, W.J. Kuai, X.T. Tao, Piezoelectricity and local structural distortions in (Na0.5Bi0.5)(1-x)SrxTiO3-Bi12TiO20 flexoelectric-type polar ceramics, Appl. Phys. Lett. 101 (2012).
[21] W. Feng Yao, H. Wang, X. Hong Xu, Y. Zhang, X. Na Yang, S. Xia Shang, Y. Hui Liu, J. Tao Zhou, M. Wang, Characterization and photocatalytic properties of Ba doped Bi12TiO20, J. Mol. Catal. A: Chem. 202 (2003) 305–311.
[22] W. Guo, S. Zhang, Y. Guo, L. Ma, F. Su, Y. Guo, A. Geng, Template-free and morphology-controlled hydrothermal growth of single-crystalline Bi12TiO20 with excellent simulated sunlight photocatalytic activity, RSC Adv. 3 (2013) 4008–4017.
[23] C. Wang, C. Shao, L. Wang, L. Zhang, X. Li, Y. Liu, Electrospinning preparation, characterization and photocatalytic properties of Bi2O3 nanofibers, J. Colloid Interface Sci. 333 (2009) 242–248.
[24] Y. Qiu, M. Yang, H. Fan, Y. Zuo, Y. Shao, Y. Xu, X. Yang, S. Yang, Nanowires of α- and β-Bi2O3: phase-selective synthesis and application in photocatalysis, CrystEngComm 13 (2011) 1843.
[25] H.T. Fan, S.S. Pan, X.M. Teng, C. Ye, G.H. Li, Structure and thermal stability of δ-Bi2O3 thin films deposited by reactive sputtering, J. Phys. D: Appl. Phys. 39 (2006) 1939–1943.
[26] A.E. Nogueira, A.R.F. Lima, E. Longo, E.R. Leite, E.R. Camargo, Structure and photocatalytic properties of Nb-doped Bi12TiO20 prepared by the oxidant peroxide method (OPM), J. Nanopart. Res. 16 (2014).
[27] C. Gao, J. Ma, Y. Sun, Z. Song, J. Fang, Z. Liu, Electrochemical Synthesis of Nanocrystalline Bi12TiO20 Powders and their Photocatalytic Ability under Visible Light, J. Am. Ceram. Soc. 94 (2011) 1336–1339.
[28] X. Sun, L. Sun, H. Zhang, J. Ma, Preparation of Visible-Light Responsive Photocatalyst (Bi20TiO32) and Its Photocatalytic Activity for Degrading Organic Pollutants, 2009, pp. 253–256.
[29] G. Zhou, H. Sun, S. Wang, H. Ming Ang, M.O. Tadé, Titanate supported cobalt catalysts for photochemical oxidation of phenol under visible light irradiations, Sep. Purif. Technol. 80 (2011) 626–634.
[30] I.V. Kityk, A. Majchrowski, J. Ebothe, B. Sahraoui, Nonlinear optical effects in Bi12TiO20 nanocrystallites embedded within a photopolymer matrix, Opt. Commun. 236 (2004) 123–129.
[31] D.L. Proffit, G.R. Bai, D.D. Fong, T.T. Fister, S.O. Hruszkewycz, M.J. Highland, P.M. Baldo, P.H. Fuoss, T.O. Mason, J.A. Eastman, Phase stabilization of δ-Bi[sub 2]O[sub 3] nanostructures by epitaxial growth onto single crystal SrTiO[sub 3] or DyScO[sub 3] substrates, Appl. Phys. Lett. 96 (2010) 021905.
[32] G. Zhong, J. Wang, Z. Zeng, The doping effects in δ-Bi2O3oxide ionic conductor,

Phys. Status Solidi (B) 245 (2008) 2737–2742.
[33] G.H. Zhong, J.L. Wang, Z. Zeng, Ionic transport properties in doped δ-Bi2O3, J. Phys.: Conf. Ser. 29 (2006) 106–109.
[34] S.L. Fu, H. Ozoe, Growth of single crystals of Bi12TiO20 from the stoichiometric melt by a floating zone method, J. Mater. Process. Manuf. Sci. 10 (2002) 127–135.
[35] J. Hou, Y. Qu, D. Krsmanovic, C. Ducati, D. Eder, R.V. Kumar, Solution-phase synthesis of single-crystalline Bi12TiO20 nanowires with photocatalytic properties, Chem. Commun. (2009) 3937–3939.
[36] S. Xu, W. Shangguan, J. Yuan, J. Shi, M. Chen, Preparations and photocatalytic degradation of methyl orange in water on magnetically separable Bi12TiO20 supported on nickel ferrite, Sci. Technol. Adv. Mater. 8 (2007) 40–46.
[37] L. Kong, H. Chen, W. Hua, S. Zhang, J. Chen, Mesoporous bismuth titanate with visible-light photocatalytic activity, Chem. Commun. (2008) 4977.
[38] W.F. Yao, H. Wang, X.H. Xu, X.N. Yang, Y. Zhang, J.T. Zhou, Y.H. Liu, S.X. Shang, M. Wang, Photocatalytic property of Zn-doped Bi12TiO20, J. Mater. Sci. Lett. 22 (2003) 989–992.
[39] S. Murugesan, Y.R. Smith, V. Subramanian, Hydrothermal synthesis of Bi12TiO20 nanostrucutures using anodized TiO2 nanotubes and its application in photovoltaics, J. Phys. Chem. Lett. 1 (2010) 1631–1636.
[40] X. Zhu, J. Zhang, F. Chen, Study on visible light photocatalytic activity and mechanism of spherical Bi12TiO20 nanoparticles prepared by low-power hydrothermal method, Appl. Catal. B: Environ. 102 (2011) 316–322.
[41] J. Hou, R. Cao, S. Jiao, H. Zhu, R.V. Kumar, PANI/Bi12TiO20 complex architectures: controllable synthesis and enhanced visible-light photocatalytic activities, Appl. Catal. B-Environ. 104 (2011) 399–406.
[42] X. Zhu, J. Zhang, F. Chen, Hydrothermal synthesis of nanostructures Bi12TiO20 and their photocatalytic activity on acid orange 7 under visible light, Chemosphere 78 (2010) 1350–1355.
[43] W.F. Yao, H. Wang, S.X. Shang, X.H. Xu, X.N. Yang, Y. Zhang, M. Wang, Photocatalytic property of Zn-modified bismuth titanate, J. Mol. Catal. A: Chem. 198 (2003) 343–348.
[44] N. Thanabodeekij, E. Gulari, S. Wongkasemjit, Bi12TiO20 synthesized directly from bismuth (III) nitrate pentahydrate and titanium glycolate and its, Powder Technol. 160 (2005) 203–208.
[45] T. Zhou, J. Hu, Mass production and photocatalytic activity of highly crystalline metastable single-phase Bi20TiO32 nanosheets, Environ. Sci. Technol. 44 (2010) 8698–8703.
[46] H. Dai, Z. Song, One-step electrochemical synthesis and visible-light photocatalytic activities of bismuth titanate coatings: effect of voltage, Ceram. Int. 41 (2015) 853–857.
[47] T. Lin, Z. Pi, M.C. Gong, J.B. Zhong, J.L. Wang, Y.Q. Chen, Gas-phase photocatalytic oxidation of benzene over titanium dioxide loaded on Bi12TiO20, Chin. Chem. Lett. 18 (2007) 241–243.
[48] S. Fu, H. Ozoe, Reaction Pathways in the Synthesis of Photorefractive gamma-Bi12MO20 (M = Si, Ge, or Ti), J. Am. Ceram. Soc. 80 (2005) 2501–2509.
[49] E.R. Camargo, E.R. Leite, E. Longo, Synthesis and characterization of lead zirconate titanate powders obtained by the oxidant peroxo method, J. Alloy. Compd. 469 (2009) 523–528.
[50] P. Francatto, F.N. Souza Neto, A.E. Nogueira, A.M. Kubo, L.S. Ribeiro, L.P. Gonçalves, L.F. Gorup, E.R. Leite, E.R. Camargo, Enhanced reactivity of peroxo-modified surface of titanium dioxide nanoparticles used to synthesize ultrafine bismuth titanate powders at lower temperatures, Ceram. Int. 42 (2016) 15767–15772.
[51] A.E. Nogueira, E. Longo, E.R. Leite, E.R. Camargo, Synthesis and photocatalytic properties of bismuth titanate with different structures via oxidant peroxo method (OPM), J. Colloid Interface Sci. 415 (2014) 89–94.
[52] A.E. Nogueira, E. Longo, E.R. Leite, E.R. Camargo, Visible-light photocatalysis with bismuth titanate (Bi12TiO20) particles synthesized by the oxidant peroxide method (OPM), Ceram. Int. 41 (2015) 12073–12080.
[53] H. Zhang, M. Lue, S. Liu, Z. Xiu, G. Zhou, Y. Zhou, Z. Qiu, A. Zhang, Q. Ma, Preparation and photocatalytic properties of sillenite Bi12TiO20 films, Surf. Coat. Technol. 202 (2008) 4930–4934.
[54] R. Chen, W. Hu, L. Zou, W. Xie, B. Li, D. Bao, Multilevel resistive switching effect in sillenite structure Bi12TiO20 thin films, Appl. Phys. Lett. 104 (2014).
[55] R. Chen, W. Hu, L. Zou, W. Xie, D. Bao, Multifunctional Eu3+-doped Bi12TiO20 thin films: resistive switching, dielectric, and photoluminescent properties, Ceram. Int. 41 (2015) S829–S834.
[56] S. Xu, W. Shangguan, J. Yuan, J. Shi, M. Chen, Preparations and photocatalytic degradation of methyl orange in water on magnetically separable Bi12TiO20 supported on nickel ferrite, Sci. Technol. Adv. Mater. 8 (2007) 40–46.
[57] D. Yu, M. Zhao, C. Wang, L. Wang, Z. Gai, C. Wang, J. Zhang, J. Li, Amorphous phases and composition dependence of piezoelectricity in BaTiO3–Bi2O3 polar amorphous ceramics, Ceram. Int. 42 (2016) 1777–1781.
[58] H. Zhang, M. Lü, S. Liu, Z. Xiu, G. Zhou, Y. Zhou, Z. Qiu, A. Zhang, Q. Ma, Preparation and photocatalytic properties of sillenite Bi12TiO20 films, Surf. Coat. Technol. 202 (2008) 4930–4934.
[59] M. Mehring, From molecules to bismuth oxide-based materials: potential homo- and heterometallic precursors and model compounds, Coord. Chem. Rev. 251 (2007) 974–1006.
[60] D. Walton, Nucleation of vapor deposits, J. Chem. Phys. 37 (1962) 2182–2188.
[61] M.J. Aziz, Film growth mechanisms in pulsed laser deposition, Appl. Phys. A 93 (2008) 579–587.
[62] A.A. Baski, H. Fuchs, Epitaxial growth of silver on mica as studied by AFM and STM, Surf. Sci. 313 (1994) 275–288.
[63] S.R. Franklin, R.K. Thareja, Monte-Carlo simulation of laser ablated plasma for thin film deposition, Appl. Surf. Sci. 177 (2001) 15–21.
[64] S. Amoruso, 6 - Plume characterization in pulsed laser deposition of metal oxide thin films, in: N. Pryds, V. Esposito (Eds.), Metal Oxide-Based Thin Film Structures, Elsevier, 2018, pp. 133–160.
[65] F. Garrelie, C. Champeaux, A. Catherinot, Study by a Monte Carlo simulation of the influence of a background gas on the expansion dynamics of a laser-induced plasma plume, Appl. Phys. A 69 (1999) 45–50.
[66] R. Castro-Rodríguez, D. Reyes Coronado, A. Iribarren, B.E. Watts, F. Leccabue, J.L. Peña, Correlation between target–substrate distance and oxygen pressure in pulsed laser deposition of complex oxide thin films, Appl. Phys. A 81 (2005) 1503–1507.
[67] H.S. Kim, H.S. Kwok, Correlation between target-substrate distance and oxygen pressure in pulsed laser deposition of YBa2Cu3O7, Appl. Phys. Lett. 61 (1992) 2234–2236.
[68] A. Melaibari, P. Molian, Pulsed laser deposition to synthesize the bridge structure of artificial nacre: comparison of nano- and femtosecond lasers, 2012.